



Lublin University
of Technology

Application of a fractional derivative in dynamical systems and structures

Grzegorz Litak

email: g.litak@pollub.pl

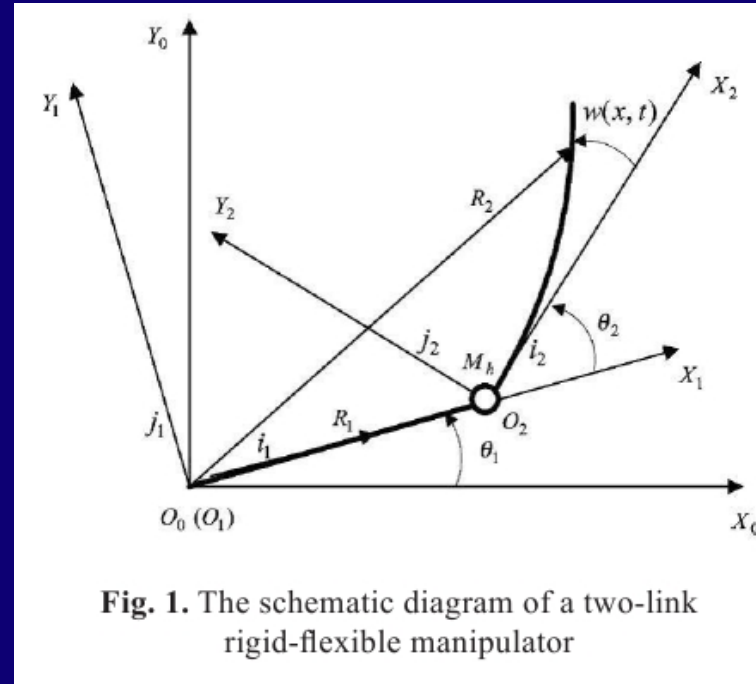
Xi'an China 2023

Outline

- Preliminaries
- Systems with fractional damping
- Broadband energy harvesting
- Diagnostics and structural health monitoring
- Synchronization of nonlinear oscillators
- Conclusions

- The concept of fractional derivatives goes back to a discussion that Leibniz and L'Hospital had over 300 years ago about the half order derivative. The problem attracted attention of many scientist (see Podlubny *Fractional Differential Equations*. San Diego: Academic Press, 1999, and Petras *Fractional-Order Nonlinear Systems: Modeling, Analysis and Simulation*. New York: Springer, 2010).
- Generally, it is assumed that the fractional order derivative is useful for a better description of real phenomena. For example,
 - * damping in mechanical devices is commonly modeled as a function (linear or nonlinear) of first order derivative (velocity) and can be replaced by fractional damping (in most cases of a composite origin). To solve a fractional differential equation, one has to approximate the corresponding derivative operator, which means including information about previous states of the system (the so-called *memory effect*).
- Fractional order introduces the effect of multiple relaxation rates. This would be positive for energy harvesting in the context of **the impedance matching principle** to get a band of possible optimum frequencies (broadening of a frequency band).

- Fractional control can be applied to a flexible manipulator which is



more safe in contact with human.

Multiple relaxation rates can introduce multiscale damping effect.

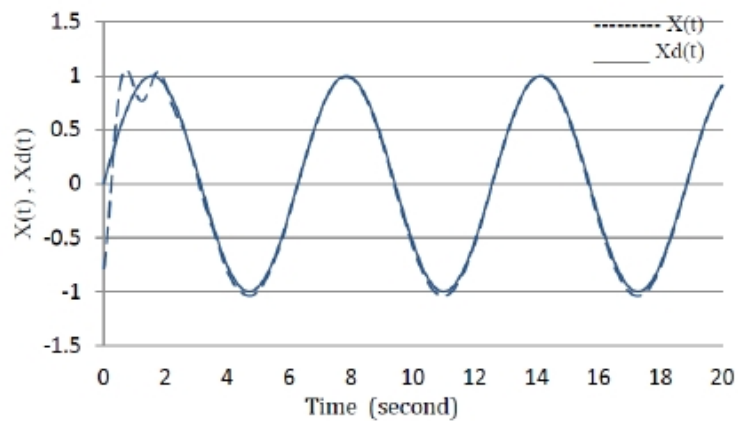


Fig. 7. Tracking response of PD sliding mode control based on Multi objective Genetic Algorithm (joint 2)

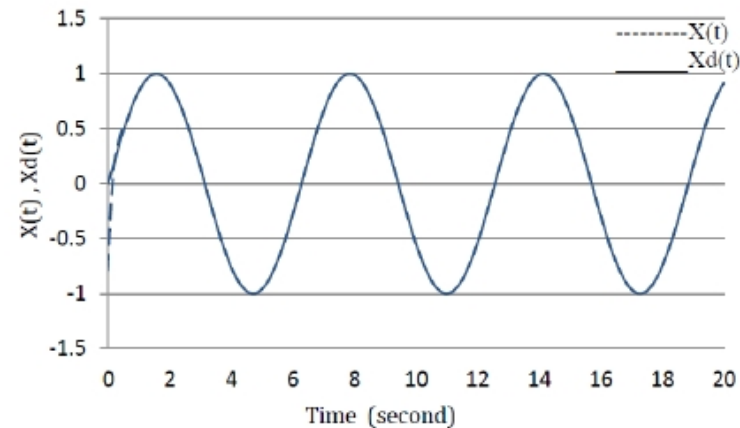


Fig. 13. Tracking response of PD^α sliding mode control based on Multi objective Genetic (joint 2)

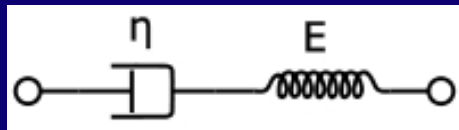
M. Pouya, P.V. Pashaki, The optimal design of fractional sliding mode control based on multi-objective genetic algorithms for a two-link flexible manipulator, *Advances in Science and Technology Research Journal* 11 (2017) 5665.

Standard descriptions of systems with multiple relaxation response

- Constitutive models of linear viscoelasticity

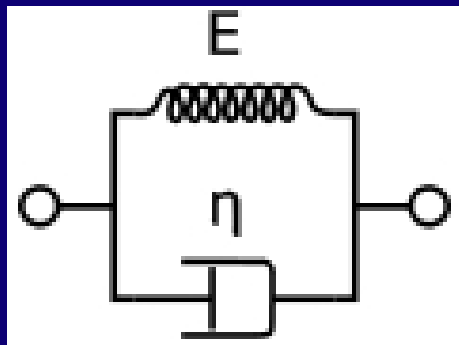
* Hook's law: $\sigma = E\varepsilon$

* Maxwell model



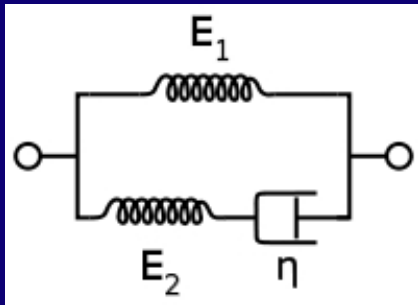
$$\frac{d\varepsilon}{dt} = \frac{d\varepsilon_D}{dt} + \frac{d\varepsilon_S}{dt} = \frac{\sigma}{\eta} + \frac{1}{E} \frac{d\sigma}{dt}$$

* Kelvin-Voigt model



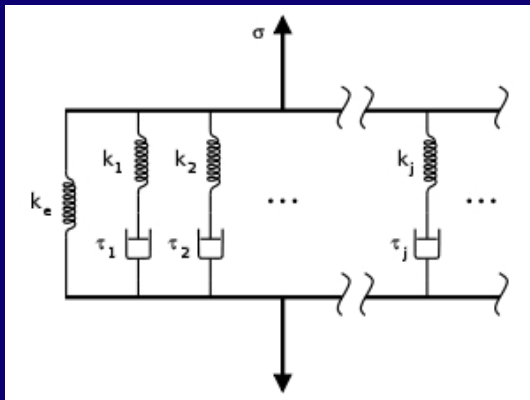
$$\sigma(t) = E\varepsilon(t) + \eta \frac{d\varepsilon(t)}{dt}$$

* Standard linear solid model



$$\frac{d\varepsilon}{dt} = \frac{E_2}{E_1 + E_2} \left(\frac{\eta}{E_2} \frac{d\sigma}{dt} + \sigma - E_1 \varepsilon \right)$$

* Generalized Maxwell Model



where multiple E_i, η_i produces the multiple relaxation time τ ($\varepsilon(t) = \varepsilon_0 e^{-\frac{t}{\tau}}$),

Alternatively, the stress-strain rate relationship can be generalized:

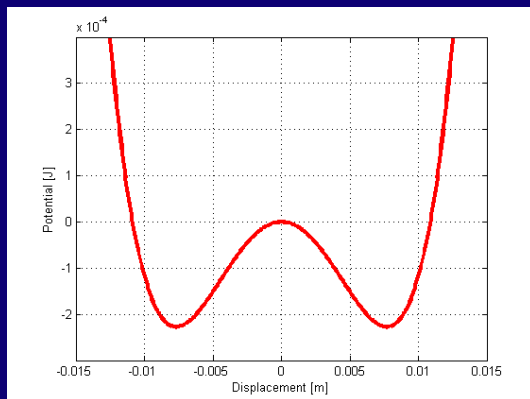
$$\sigma = \eta \frac{d\varepsilon}{dt} \rightarrow \sigma = \eta \frac{d^q \varepsilon}{dt^q} \quad \text{with a fractional order } q$$

- Fractional derivative is introduced to describe the system with multiple relaxation times. This derivative can be expressed as a combination of conventional (of integer order) integral and derivative. It is linear but introduces the memory (or history of evolution or hysteresis if additional nonlinearities are present) to the description of the system state.
- Simultaneously, it also introduces additional degrees of freedom. Such multidimensional dynamical systems meet difficulties in nonlinear analysis and require a special treatment for analysis of the dynamical response of a system including nonperiodic solutions or chaos detection.

We start with the standard well known nonlinear Duffing equation:

$$\frac{d^2x}{dt^2} + \alpha \frac{dx}{dt} - x + x^3 = \delta \cos(\omega t)$$

where $\alpha \geq 0$ denotes the damping coefficient, δ denotes the amplitude and ω denotes the frequency of external excitation. The model describes the dynamics of a mass in a double potential well and exhibits chaotic behaviour.



To introduce a fractional derivative to the dynamical system, the widely used **Grünwald-Letnikov** and **Riemman-Liouville** definitions are applied. Both of them are particular cases of a general fractional order operator - namely, the former represents the q order derivative, while the later represents the q fold integral. In this sense, the class of functions described by the Riemman-Liouville definition is broader (function must be integrable) than the one defined by Grünwald and Letnikov (function must be $m + 1$ continuously differentiable). However, for a function of the Grünwald - Letnikov class, both definitions are equivalent.

Introducing the first order derivative, we will briefly demonstrate the idea of noninteger derivative. Let us consider the first and second order derivative:

$$\begin{aligned}f'(t) &= \lim_{h \rightarrow 0} \frac{f(t) - f(t-h)}{h} \\f''(t) &= \lim_{h \rightarrow 0} \frac{f'(t) - f'(t-h)}{h} \\&= \lim_{h \rightarrow 0} \frac{f(t) - 2f(t-h) + f(t-2h)}{h^2}\end{aligned}$$

Continuing, one can write a general form of the n -th order derivative:

$$f^n(t) = \lim_{h \rightarrow 0} \frac{1}{h^n} \sum_{j=0}^n (-1)^j \binom{n}{j} f(t-jh) \quad n \in \mathbb{N}$$

In analogy to the original Newton expansion

$$(x+y)^r = \sum_{k=0}^{\infty} \binom{r}{k} x^k y^{r-k}.$$

$$f^n(t) = \lim_{h \rightarrow 0} \frac{1}{h^n} \sum_{j=0}^{\infty} (-1)^j \binom{n}{j} f(t - jh) \quad n \in \mathbb{N}$$

which leads to the Grünwald - Letnikov definition:

$$\begin{aligned} \frac{d^q f}{dt^q} &\equiv_L D_t^q f(t) \\ &= \lim_{h \rightarrow 0} \frac{1}{h^q} \sum_{j=0}^{\lceil \frac{t-a}{h} \rceil} (-1)^j \binom{q}{j} f(t - jh), \end{aligned}$$

where $q > 0$ and the binomial coefficients can be extended to real numbers using the Euler Gamma function

$$\binom{q}{j} = \frac{q!}{j!(q-j)!} = \frac{\Gamma(q+1)}{\Gamma(j+1)\Gamma(q-j+1)};$$

a pair of square brackets $[\cdot]$ appearing in the upper limit of the sum denotes the integer part, while L is the length of the memory, respectively.

According to the short memory principle (Podlubny 1999, Petras 2010), the length of system memory can be substantially reduced in the numerical algorithm to get reliable results. Thus, the derivative can be expressed

$${}_L D_t^q f(t) = \lim_{h \rightarrow 0} \frac{1}{h^q} \sum_{j=0}^{[N(t)]} (-1)^j \binom{q}{j} f(t - jh),$$

where $N(t) = \min(\frac{t-L}{h}, \frac{L}{h})$. Note that by this choice we do not need initial conditions before $t = 0$, as is usually required for other systems with memory. Now, the Duffing system with a fractional damping term has the following form:

$$\frac{d^2 x}{dt^2} + \alpha \frac{d^q x}{dt^q} - x + x^3 = \delta \cos(\omega t)$$

Last equation can be decomposed into a set of equations of lower degree:

$$\begin{aligned} {}_L D_t^1 x(t) &= y(t) \\ {}_L D_t^q x(t) &= w(t) \\ {}_L D_t^1 y(t) &= x(t) + \alpha w(t) - x^3(t) + \delta \cos(\omega t) \end{aligned}$$

The set of equations can be written in the discretized form by the following fractional order Newton-Leipnik algorithm (Petras 2010):

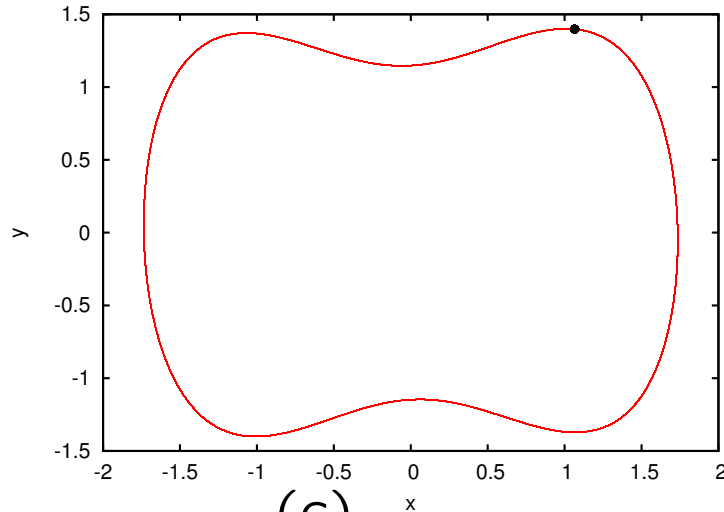
$$\begin{aligned}
 x(t_k) &= x(t_{k-1}) + y(t_{k-1})h \\
 x(t_k) &= w(t_{k-1})h^q - \sum_{j=1}^{N-1} c_j^{(q)} x(t_{k-j}) \\
 y(t_k) &= y(t_{k-1}) + [\alpha w(t_{k-1}) - x^3(t_{k-1}) \\
 &\quad + \delta \cos(\omega(t_{k-1}))]h,
 \end{aligned}$$

where h is the integration step and the coefficients $c_j^{(q)}$ satisfy the following recursive relations:

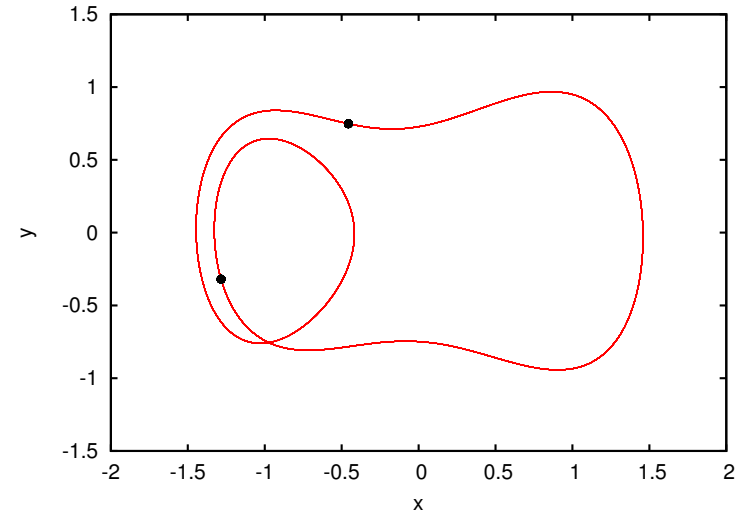
$$c_0^{(q)} = 1, \quad c_j^{(q)} = \left(1 - \frac{1+q}{j}\right) c_{j-1}^{(q)}.$$

Solution identification

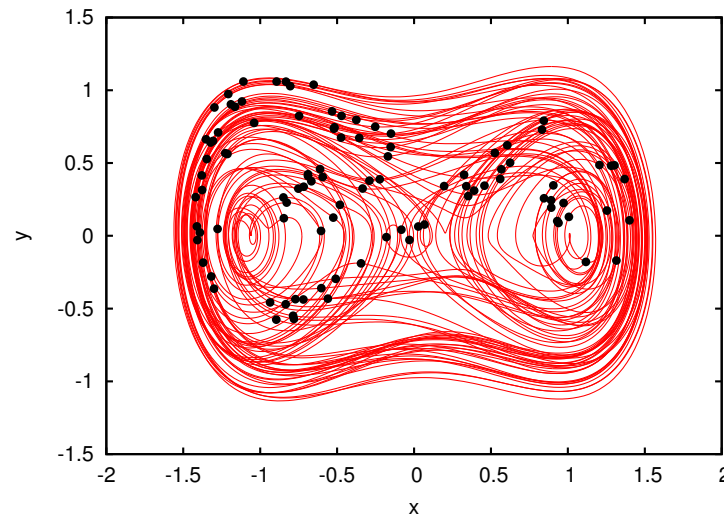
(a)



(b)

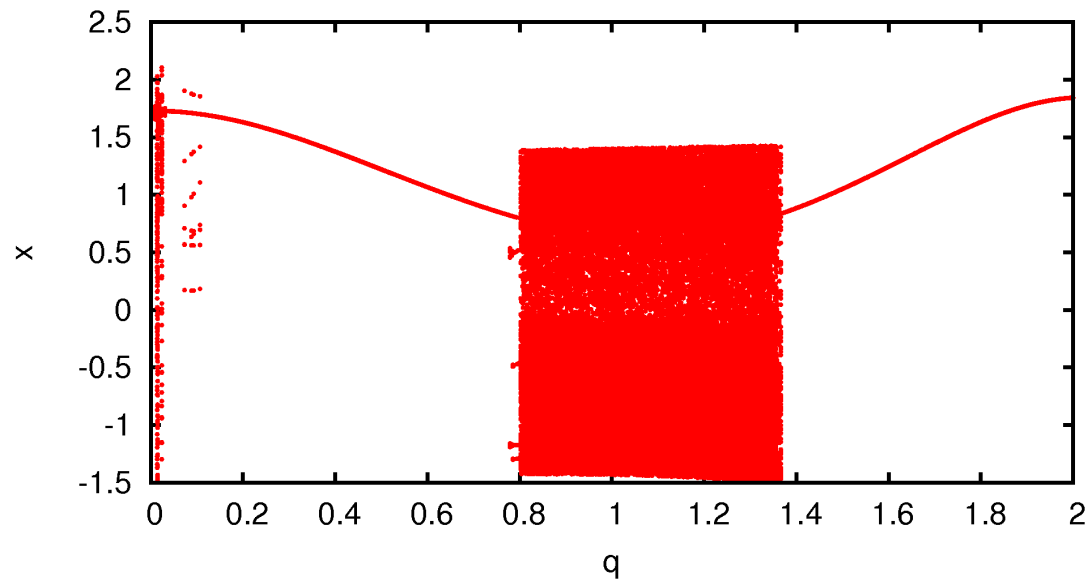


(c)

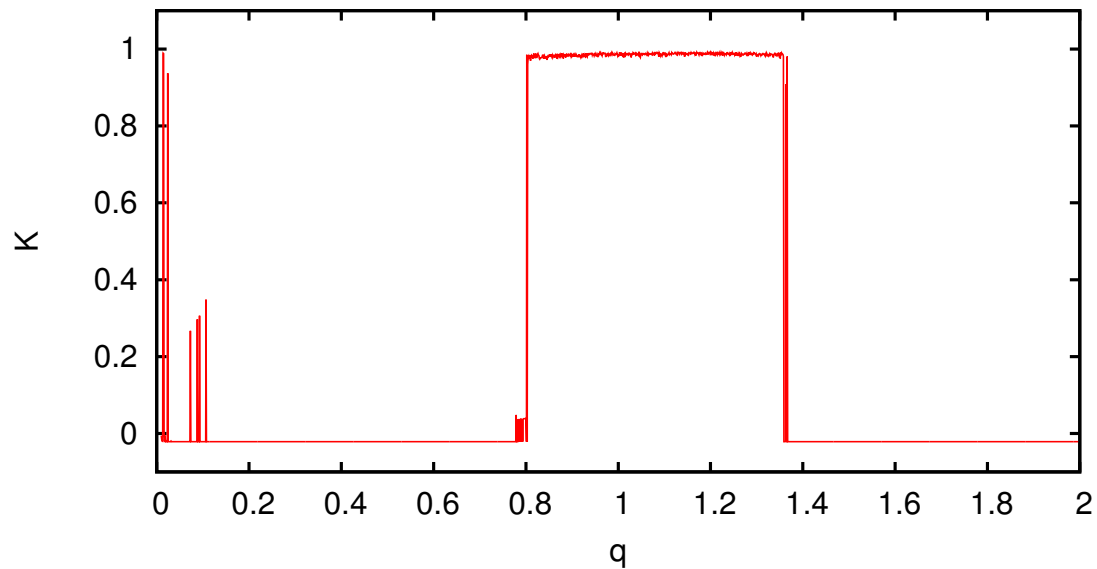


(Syta *et al.* Chaos
24, 013107, 2014)

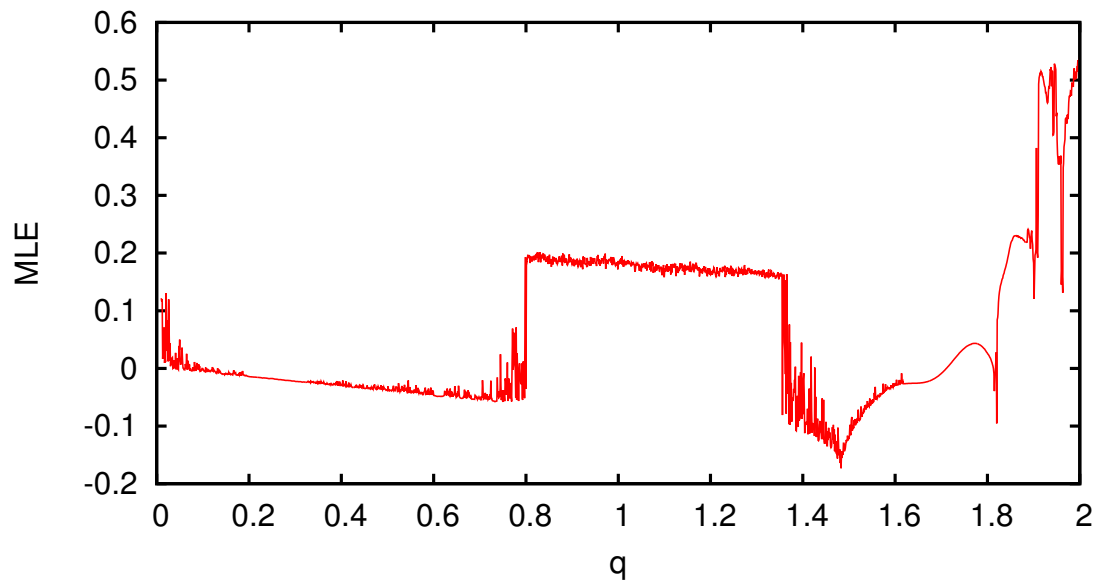
The phase portraits and Poincaré points for the period one numerical solution (a), with $q = 0.6$; the period two numerical solution (b) with $q = 0.8$; the chaotic numerical solution with $q = 1.0$. Other parameters $\alpha = 0.15$, $\delta = 0.3$ and $\omega = 1.0$ and the initial conditions $(x_0, y_0) = (0.2, 0.3)$.



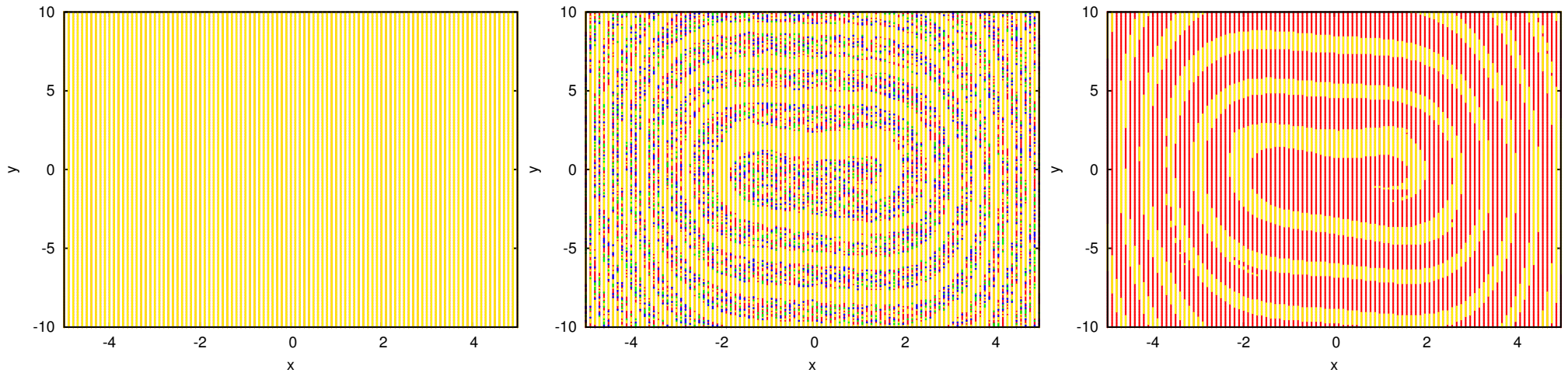
The bifurcation diagram of the x coordinate versus the order of the derivative $q \in [0.01, 2.0]$; $\Delta q = 0.001$ and initial conditions for each q were $(x_0, y_0) = (0.2, 0.3)$. Other system parameters are: $\alpha = 0.15$, $\delta = 0.3$, and $\omega = 1.0$.



(Test 0-1 for chaotic solutions) K versus q with the sampling $\Delta q = 0.001$, the initial conditions for each q were: $(x_0, y_0) = (0.2, 0.3)$. Other system parameters: $\alpha = 0.15$, $\delta = 0.3$, and $\omega = 1.0$.



Maximal Lyapunov Exponent as a function of the fractional order $q \in [0.01, 2.0]$ and $\Delta q = 0.001$. The distance between neighbouring trajectories has been estimated in one tenth of the excitation period interval T ($T = 2\pi/\omega$). Other system parameters: $\alpha = 0.15$, $\delta = 0.3$, and $\omega = 1.0$.



(a)

(b)

(c)

I Basins of attraction (a) for $q = 0.6$ (the uniform colour covering the whole region of initial conditions corresponds to the global period one regular solution); (b) for $q = 0.8$ (the colours denote the interplay of four different solutions, yellow - denotes the period one regular solution; green and blue - two different period two solutions; red - non-periodic (chaotic) solution); (c) for $q = 1.0$ (the colours denote different solutions, yellow - denotes the period one regular solution while red - non-periodic (chaotic) solution).

Properties of the fractional system

- The fractional order of damping introduces memory effects that extend the dimension of the phase space. As a consequence of an uncertainty in the dynamical system dimension, the maximal Lyapunov exponent values may not correspond to the properties of the attractor. In that case, the 0-1 method appeared to give more adequate results.
- We also found sensitivity to initial condition in the considered system. Interestingly, different values of the order of damping change dramatically the basins of attraction: from one attractor (periodic) to four attractors (periodic, two different period two solutions and none-periodic) exhibiting Wada basins, and finally, to two attractors (period one and non-periodic).
- One should note that any system with a fractional derivative is characterized by long transient intervals appearing before reaching the stationary state. This property complicates the investigation of the system dynamics. We would like to stress that our results for dynamics of the system were obtained after cutting off the corresponding long transients.

Dynamics of the fractionally damped broadband piezoelectric energy generator

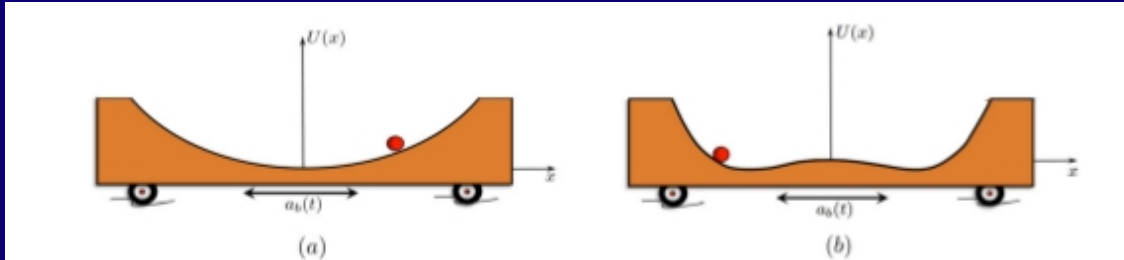


Fig. 5 The dynamics of a nonlinear energy harvester can be fairly well understood via a simple analogy with a particle moving along a cart. (a) Monostable potential and (b) bistable potential.

BROAD BAND EFFECT

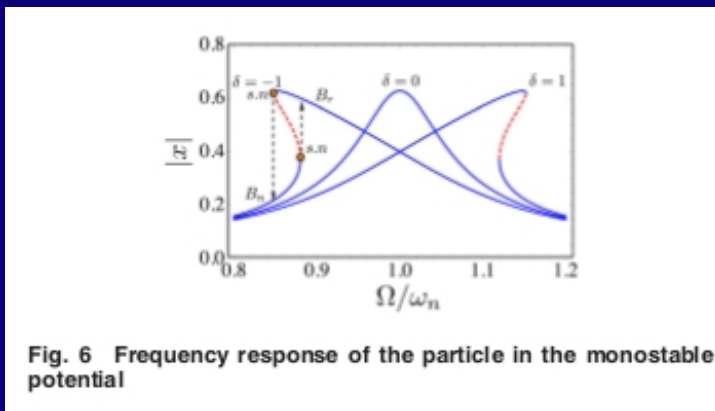
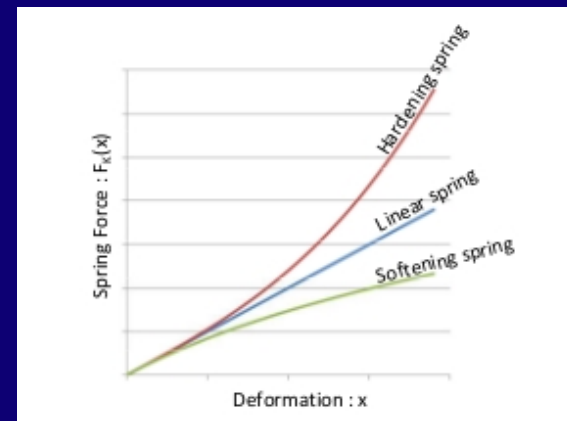


Fig. 6 Frequency response of the particle in the monostable potential



MF Daqaq, R Masana, A Erturk, DD Quinn, On the Role of Nonlinearities in Vibratory Energy Harvesting: A Critical Review and Discussion, Applied Mechanics Reviews 66, 040801 (2014)

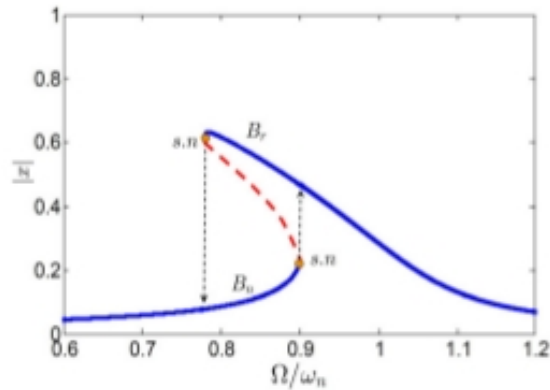


Fig. 10 Frequency response of the particle in a single potential well of the bistable potential system when $A < A_1$. Dashed lines represent unstable periodic responses.

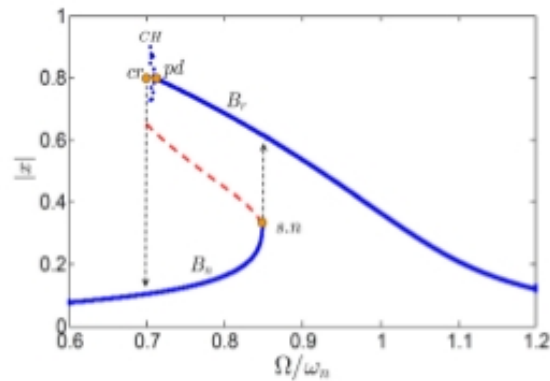


Fig. 11 Frequency response of the particle in a single potential well of the bistable potential system when $A_1 < A < A_2$. Dashed lines represent unstable periodic responses.

MF Daqaq, R Masana, A Erturk, DD Quinn, Applied Mechanics Reviews 66, 040801 (2014)

In the present model we considered the vertical flexible beam with fractional damping and nonharmonic potential dependent on the magnets orientation angle. The differential equations reads:

$$M\ddot{z}(t) + CD^\alpha z(t) + Kz(t) + F_m - \Theta u(t) = F_e$$

$$C_p \dot{u}(t) + \Theta z(t) + R^{-1}v(t) = 0.$$

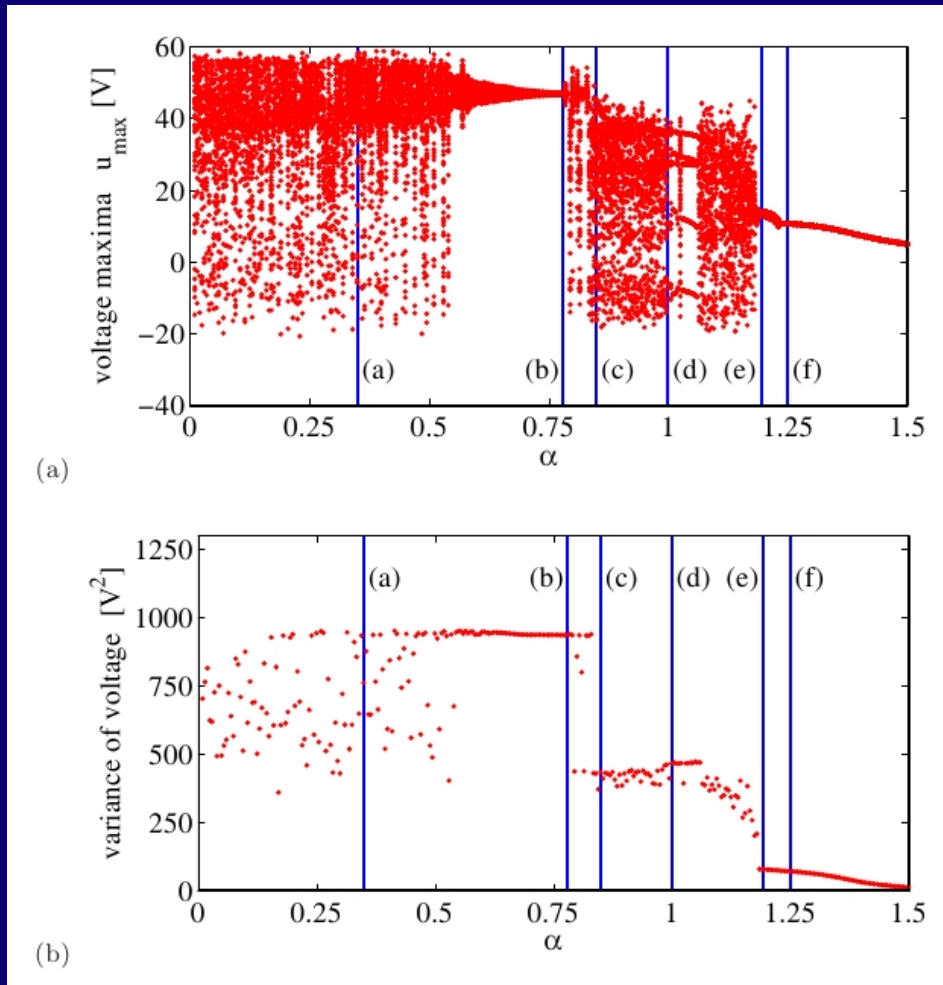
There the system parameters have been identified from the experimental : $M = 0.0061\text{kg}$; $C = 0.02467633\text{Ns/m}$; $K = 63.7633\text{N/m}$; $\Theta = 9.1908212 \times 10^{-5}\text{N/V}$ and other parameters after. The F_m is the magnetic force, while F_e excitation harmonic force $F_e/M = A\sin(2\pi ft)$. In the following simulations we used the fixed $A = 0.56g$, where g is the gravitational acceleration, and $f = 10\text{Hz}$.

The nonlinear magnetic force expanded as a polynomial:

$$F_m = a_0 + a_1 z(t) + a_2 z^2(t) + \dots + a_n z^n(t),$$

where $a_0 = 0$, $a_1 = 79.1661$; $a_2 = 0$; $a_3 = -2.6078 \times 10^5$ for zero of the inclination angle of external magnets.

Simulation results and discussion



The fractional order of damping makes the significant changes in the system response. The system goes through several bifurcations with changing α .

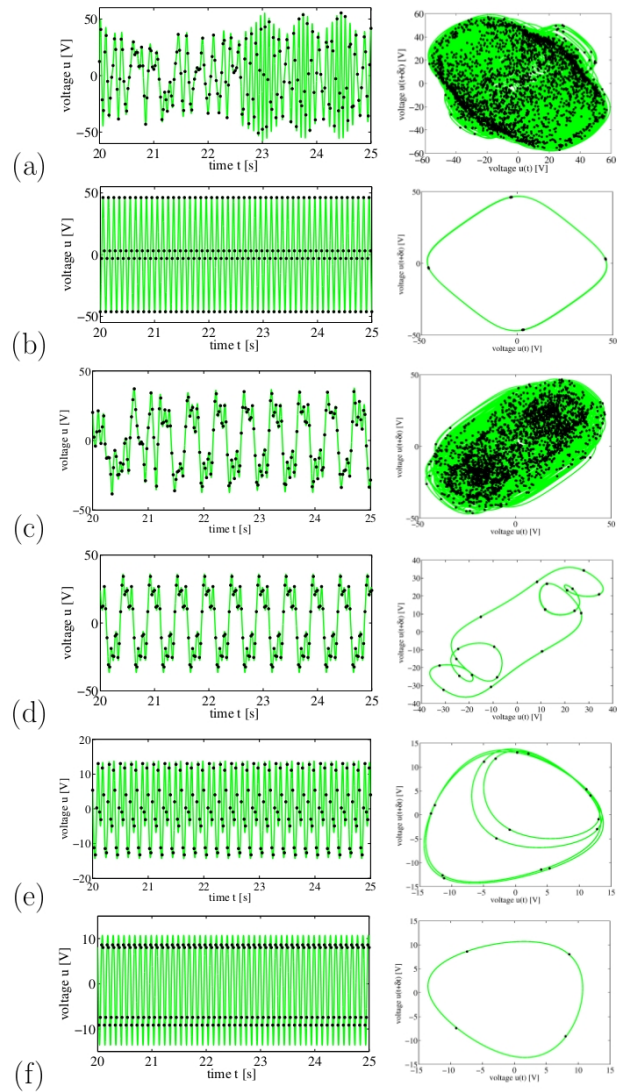


Figure 3: Voltage open circuit time series and the corresponding phase portrait with delayed coordinate (delay was fixed to one quarter of excitation period) for $\alpha = 0.35, 0.78, 1.00, 1.195, 1.25$ for a-f, respectively.

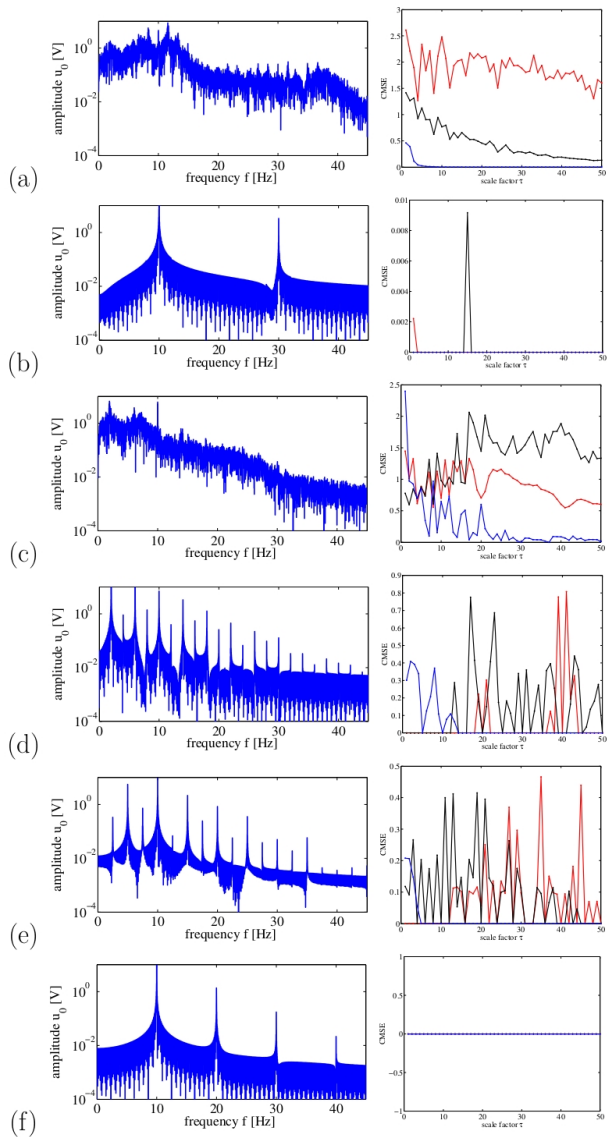


Figure 4: Fourier spectra and Multiscale Entropy CMSE for $\alpha = 0.35, 0.78, 1.00, 1.195, 1.25$ for a-f, respectively. The results of CMSE for $m = 2$ (length of the chain) and three values of the similarity factor r ($r = 0.01\sigma_u$ - red line, $0.1x$ - black line, and $1x$ - blue line). Note that oscillations of CMSE between large and nearly zero values or permanent zero value (for all lines) signal regular solution. Otherwise the solution is chaotic (as Figs. a and c).

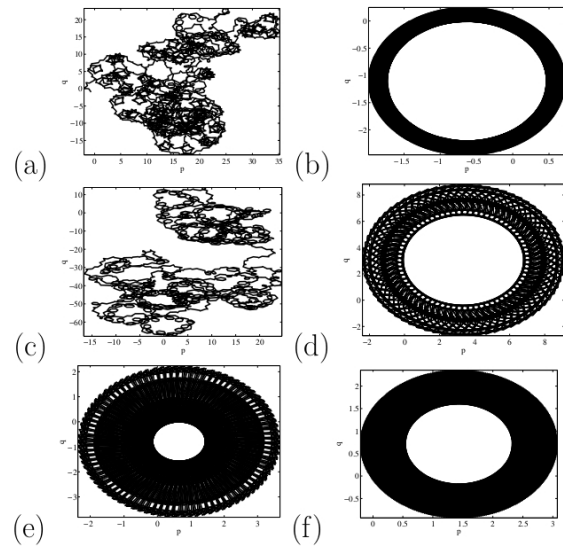


Figure 5: 0-1 test results. Phase portraits in (p, q) units $K = 0.993, -0.005, 0.994, 0.000, -0.005, -0.004$ for Fig. 5a-f. Note that the asymptotic value of the parameter $K \rightarrow 0$ for regular motion and $K \rightarrow 1$ for chaos (cases a and c).

Fractional order for machine diagnostics and structural health monitoring

Advanced signal processing

The diagram illustrates the relationship between different orders of derivation and their corresponding physical quantities and fault types. It shows a horizontal axis labeled 'Order of derivation' with points 0, 1, 2, 3, and 4. Above the axis, 'Displacement $x^{(0)}$ ' is at 0, 'Velocity $x^{(1)}$ ' is at 1, 'Acceleration $x^{(2)}$ ' is at 2, and 'Higher order derivatives $x^{(n)}$ ' are indicated for 3 and 4. Below the axis, two lists of fault types are provided: one for orders 0-2 and another for orders 3-4.

- Unbalance
- Misalignment
- Bent shaft
- Mechanical looseness
- Resonance

- Bearing fault
- Cavitation
- Damaged or worn gears
- Insufficient lubrication
- ...

$$\frac{dx}{dt} = x^{(1)} = \omega X \sin(\omega t + \frac{\pi}{2}),$$

Real order
$$\frac{d^\alpha x}{dt^\alpha} = x^{(\alpha)} = \omega^\alpha X \sin(\omega t + \alpha \frac{\pi}{2}) = X_\alpha \sin(\omega t + \varphi_\alpha), \quad \rightarrow \text{Improved sensitivity}$$

CM 2009 – MFPT 2009
 Dublin, Ireland, June 23-25, 2009

UNIVERSITY of OULU
 OULUN YLIOPISTO

invented by prof. Sulo Lahdelma (Oulu, Finland)

FEATURES IN FAULT DETECTION

© Professor Sulo Lahdelma 2008 | <https://lahdelma.wordpress.com>

NATURE OF FAULT	SIGNAL	FEATURES
1. Unbalance	$x, x^{(1)}$	rms, p
2. Misalignment	$x, x^{(2)}$	rms, p
3. Bent shaft	$x, x^{(1)}$	rms, p
4. Damaged rolling element bearings	$x^{(2)}, x^{(3)}, x^{(4)}, x^{(\alpha)}, \alpha > 2$	rms, p, cf, k, l_p -norm
5. Mechanical looseness	$x, x^{(1)}, x^{(2)}, x^{(3)}, x^{(4)}$	rms, p
6. Damaged or worn gears	$x^{(2)}, x^{(3)}, x^{(4)}$	rms, p, l_p -norm
7. Oil whirl	$x^{(\alpha)}, \alpha < 0, x, x^{(1)}$	rms, p
8. Cavitation	$x^{(2)}, x^{(3)}, x^{(4)}$	rms, p, k, l_p -norm
9. Electrical problems	$x, x^{(1)}, x^{(2)}$	rms, p
10. Loose stator coils	$x^{(2)}, x^{(3)}, x^{(4)}$	rms, p
11. Resonance	$x, x^{(1)}$	rms, p
12. Poor lubrication	$x^{(2)}, x^{(3)}, x^{(4)}$	rms, p, l_p -norm
13. Roll surface defects	$x, x^{(1)}, x^{(2)}$	rms, p
14. Lime kiln: misalignment and damaged supporting rolls	$x^{(2)}, x^{(3)}, x^{(4)}$	p
	<p>x displacement $x^{(1)}$ velocity $x^{(2)}$ acceleration $x^{(3)}$ jerk $x^{(4)}$ snap $x^{(\alpha)}$ real number α is the order of derivative</p>	<p>rms root mean square p peak value cf crest factor k kurtosis</p> <p>Features e.g. for displacement: x_{rms}, x_p, x_{cf} and x_k</p> <p>$\ x\ _p$ l_p-norm for displacement</p>

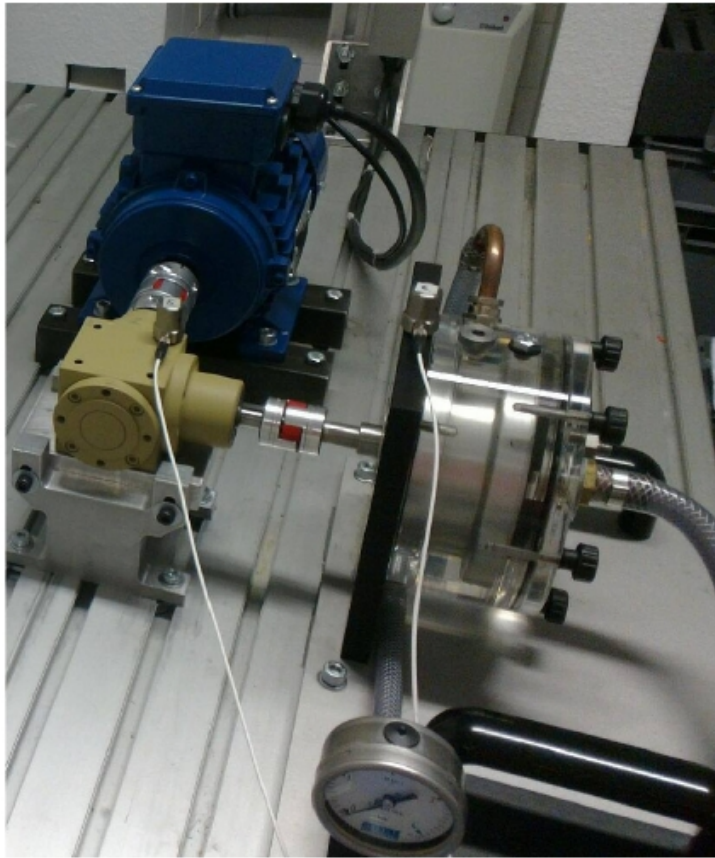


Figure 1. The testing equipment consisting of electric motor, bevel gear and pump

K. Karioja, S. Lahdelma, G. Litak, B. Ambrozkiewicz, Extracting periodically repeating shocks in a gearbox from simultaneously occurring random vibration, In: [Fifteenth International Conference on Condition Monitoring and Machinery Failure Prevention Technologies \(CM 2018/MFPT 2018\)](#), 2018, pp. 456-464.

The test equipment consisted of:

Bodywork of G.U.N.T. PT 500 test rig

1.1 kW electric motor manufactured by EMK

Nordac 700E frequency converter

Mdler 41200102 bevel gearbox with transmission ratio 1:2 ($z_1 = 54, z_2 = 27$)

Centrifugal pump with 3 blades on impeller for cavitation testing, manufactured by G.U.N.T.

2 KTR claw clutches, with 4 claws on flexible elements

Enveloping is often utilised when aiming to detect periodically repeating shocks from vibration measurements. In following envelope is created by first band pass filtering the signal, then rectifying it and low pass filtering the resulting signal. Enveloping is a common method in condition monitoring. However, it is rarely applied to any other signals than acceleration or velocity. This may be adequate way, but there are more possibilities.

It is a generally accepted fact that a cracked tooth in a gear causes a shock once a revolution of the gear. In this case it means the shock is expected to occur at a frequency of 66.67 Hz. Distinguishable peaks at that frequency and its multiples are considered a sign of this type of fault.

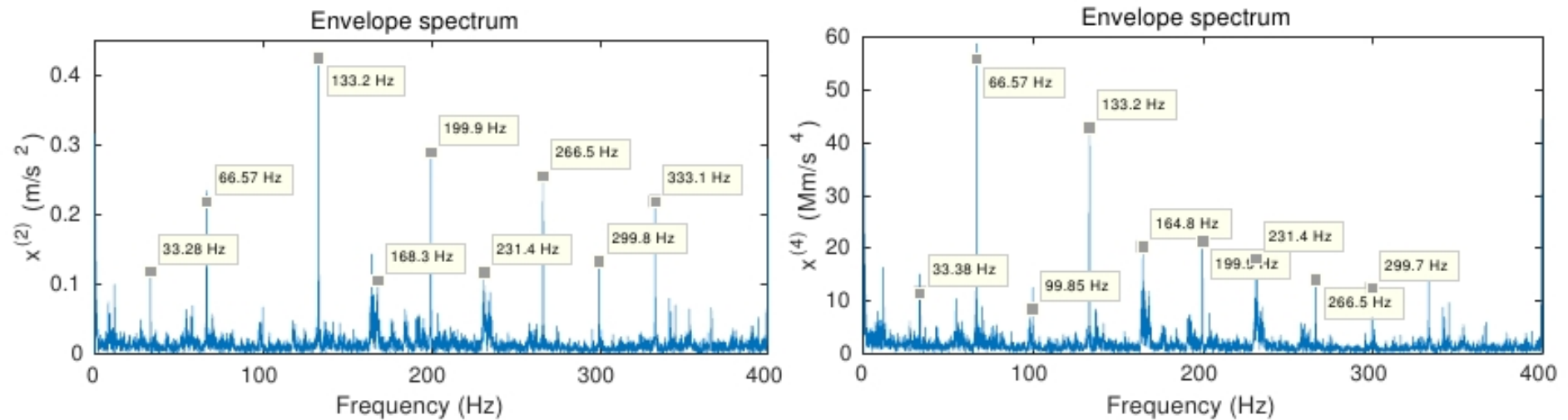


Figure 4. Envelope spectra of acceleration and snap from the gearbox when cavitation occurs, band pass filtering from 1000 Hz to 2000 Hz

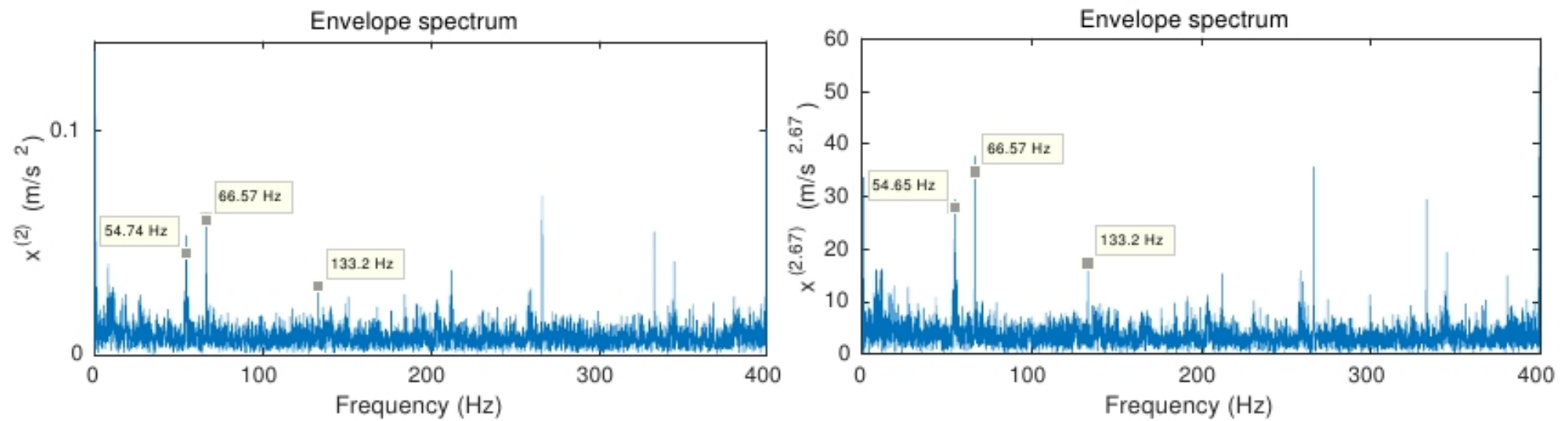


Figure 5. Envelope spectra of acceleration and $x^{(2.67)}$ from the pump when cavitation occurs, band pass filtering from 1000 Hz to 2000 Hz

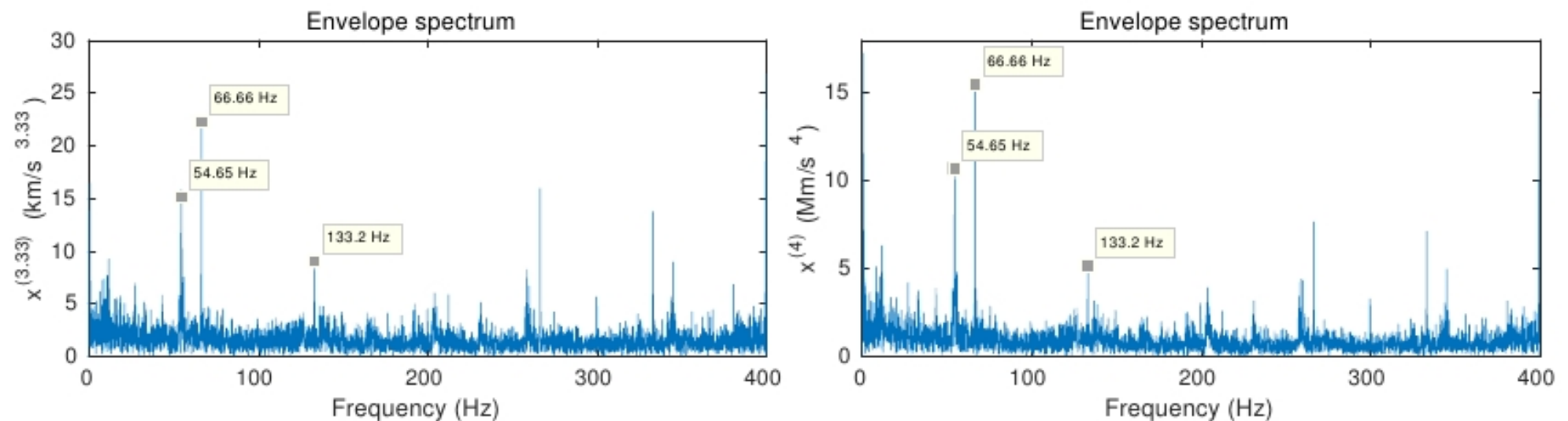


Figure 6. Envelope spectra of $x^{(3.33)}$ and snap from the pump when cavitation occurs, band pass filtering from 1000 Hz to 2000 Hz

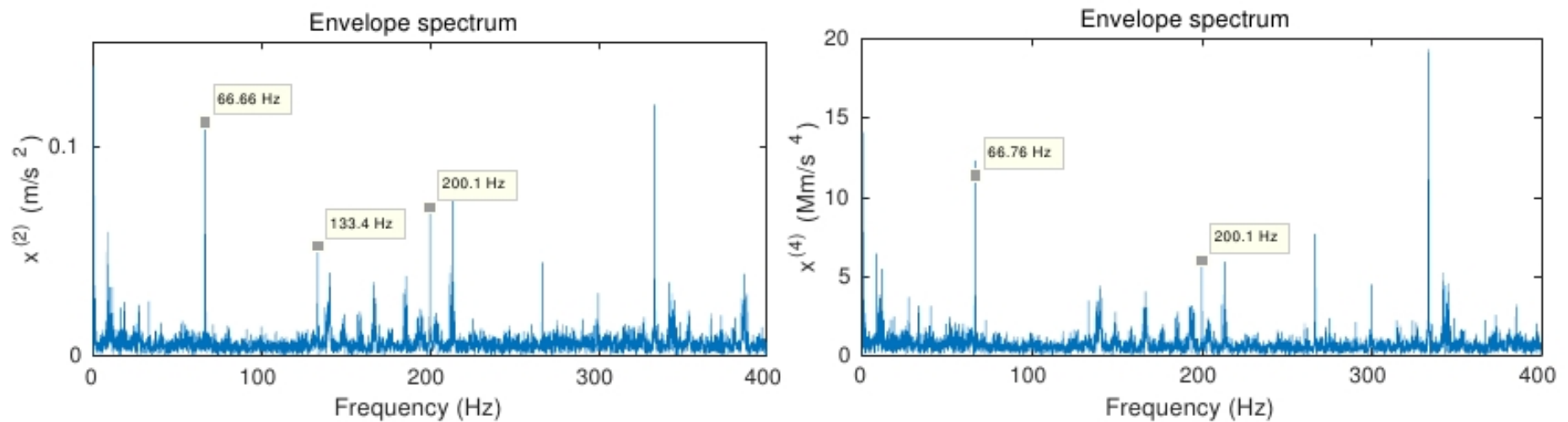


Figure 7. Envelope spectra of acceleration and snap from the pump without cavitation, band pass filtering from 1000 Hz to 2000 Hz

The Hilbert transform of the considered signal $x(t)$ is defined by an integral transform [Feldman 2011, Wang 2016]:

$$H[x(t)] = H_1[x(t)] = \frac{1}{\pi} \int_{-\infty}^{\infty} \frac{x(\tau)}{t - \tau} d\tau,$$

where H_1 denotes the conventional *integer* Hilbert transform.

Its extension to the *fractional* Hilbert transform is given [Wanf 2016] by the formula:

$$H_p[x(t)] = \cos(p\pi/2)H_0[x(t)] + \sin(p\pi/2)H_1[x(t)],$$

where $H_0[x(t)] = x(t)$.

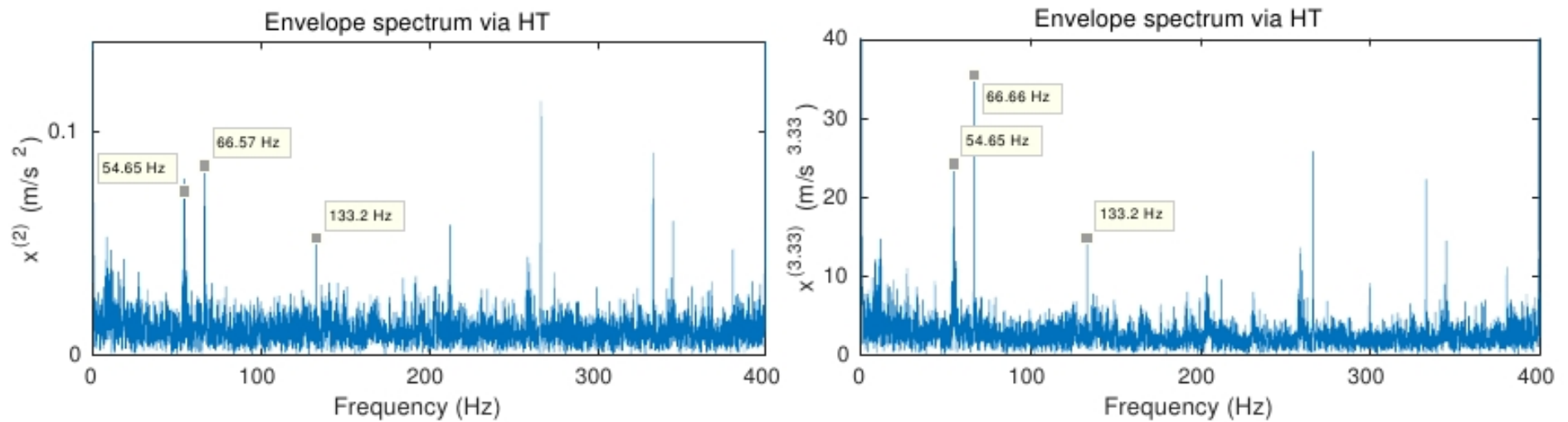


Figure 8. Envelope spectra of acceleration and $x^{(3.33)}$ obtained via Hilbert transform from the pump when cavitation occurs, band pass filtering from 1000 Hz to 2000 Hz

Fractional order for synchronization

- R Kengne, R Tchitnga, A Mezatio, A Fomethe, G Litak, Finite-time synchronization of fractional-order simplest two-component chaotic oscillators European Physical Journal B 90, 88, 2017
- Fractional-order two-component oscillator: stability and network synchronization using a reduced number of control signals R Kengne, T Robert, SAK Tewa, G Litak, F Anaclet, C Li, European Physical Journal B 91, 304, 2018

is investigated under consideration of the following master system

$$\left\{ \begin{array}{l} \frac{d^q V_{GS}^m}{dt^q} = \frac{1}{C_{GS}} (-i_1^m + i_2^m - i_D^m - I_d^m) \\ \frac{d^q V_{GD}^m}{dt^q} = \frac{1}{C_{GD}} (-i_2^m + I_d^m) \\ \frac{d^q i_1^m}{dt^q} = \frac{1}{L_1} V_{GS}^m \\ \frac{d^q i_2^m}{dt^q} = \frac{1}{L_2} (-V_{GS}^m + V_{GD}^m + E) \end{array} \right. \quad (4)$$

and the corresponding slave system:

$$\left\{ \begin{array}{l} \frac{d^q V_{GS}^s}{dt^q} = \frac{1}{C_{GS}} (-i_1^s + i_2^s - i_D^s - I_d^s \\ \quad - \xi \text{sign}(V_{GS}^s - V_{GS}^m) - \xi u(t)) \\ \frac{d^q V_{GD}^s}{dt^q} = \frac{1}{C_{GD}} (-i_2^s + I_d^s) \\ \frac{d^q i_1^s}{dt^q} = \frac{1}{L_1} V_{GS}^s \\ \frac{d^q i_2^s}{dt^q} = \frac{1}{L_2} (-V_{GS}^s + V_{GD}^s + E). \end{array} \right. \quad (5)$$

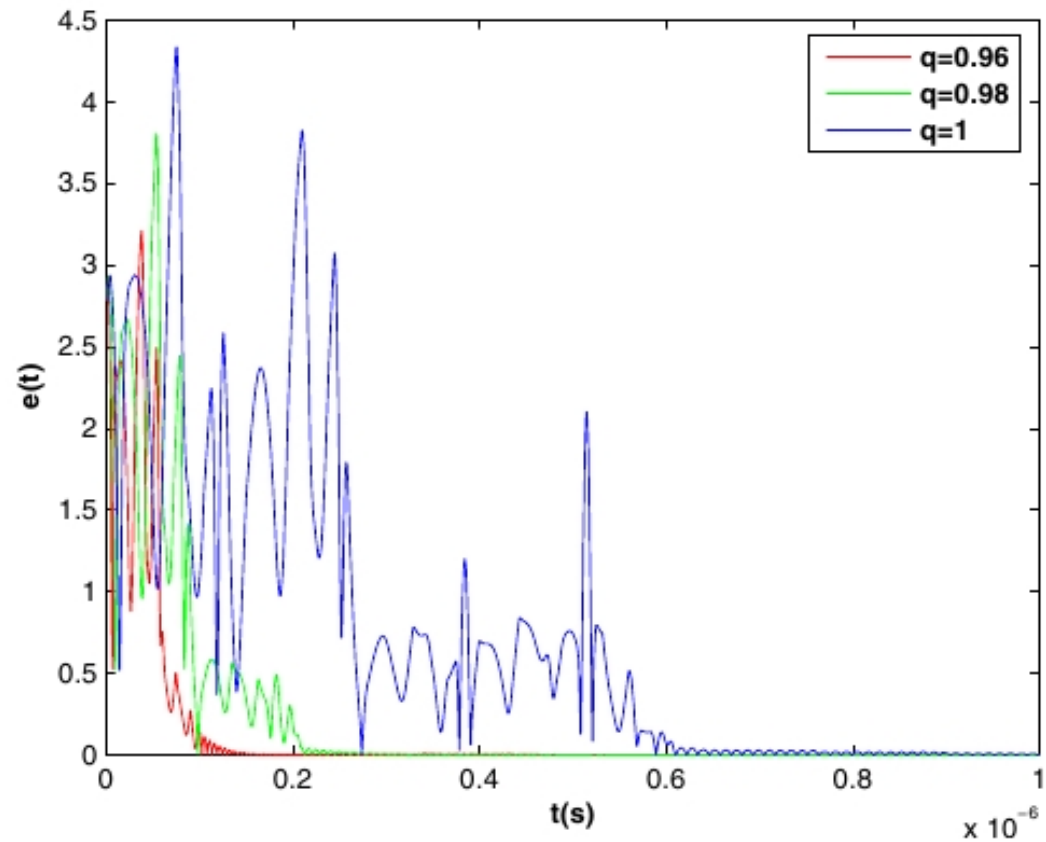


Fig. 6. Time evolution of synchronization errors $e(t) = \sqrt{e_1^2 + e_2^2 + e_3^2 + e_4^2}$ for different values of fractional-order $q = 1$ (blue), $q = 0.98$ (green), and $q = 0.96$ (red) when the bias voltage source is kept at $E = 4$ V. It can be noted that the numerical finite-time of synchronization decreases with the fractional-order.

Conclusions

- The fractional derivative is introduced to describe multiple relaxation times in viscoelastic material properties. Usually, fractional derivative modelling reduce the model degree of freedom. This can lead to some confusion in states description and/or their identification.
- The fractional derivative enables to adjust the best variable to detect the failures in the dynamical structures. This could be important as many variables, which are obtained in experiments are projected or transformed. Fractional derivation restores the information about the failures in the dynamical structures.

- An efficient finite-time adaptive controller with fractional properties was introduced. It was shown that the synchronization of fractional-order systems is faster than that of integer ones. We also proposed an application of such a schema to cryptography.